Applied Surface Science 665 (2024) 160338

Contents lists available at ScienceDirect

Applied Surface Science

journal homepage: www.elsevier.com/locate/apsusc

Full Length Article

Antibacterial property alterations induced by low zinc content in laser-structured brass

Aisha Saddiqa Ahmed [a,b,*], Daniel Wyn Müller [a], Stéphanie Bruyère [b], Anne Holtsch [c], Frank Müller [c], Kristina Brix [d], Sylvie Migot [b], Ralf Kautenburger [d], Karin Jacobs [c], Jean–François Pierson [b], Frank Mücklich [a]

[a] Chair of Functional Materials, Department of Material Science and Engineering, Saarland University, 66123 Saarbrücken, Germany
[b] Université de Lorraine, CNRS, IJL, F-54000 Nancy, France
[c] Experimental Physics and Center for Biophysics, Saarland University, 66123 Saarbrücken, Germany
[d] Department of Inorganic Solid-State Chemistry, Elemental Analysis, Saarland University, 66123 Saarbrücken, Germany

ARTICLE INFO

Keywords:
Femtosecond pulsed direct laser interference patterning
Brass
Nanoscale modification
Antibacterial
Bacteria-substrate contact
Escherichia coli

ABSTRACT

Brass, along with other copper-based alloys, exhibits advantageous antibacterial properties that can be further enhanced by altering the surface topography to increase bacterial adhesion. This enhancement is achievable through a higher contact area created by precise periodic structures, each approximately the size of a single bacterial cell. One method for generating these structures is ultrashort pulsed direct laser interference patterning (USP-DLIP). However, this process may induce chemical alterations in addition to topographical changes, depending on the substrate's composition. To mitigate unfavorable chemical alterations, brass with a 15% zinc content was selected for this study. The antibacterial effectiveness of the modified surfaces was tested against *Escherichia coli*, providing initial insights into the interaction between bacteria and the substrate. The results indicate that modified brass with a 15% zinc content shows improved antibacterial activity. Overall, this research demonstrates that by modifying a surface with the appropriate chemical composition, effective bacterial elimination through contact can be achieved.

1. Introduction

Excessive consumption of antibiotics over the last few decades has created multidrug resistance among several pathogens. The spread of such pathogens has resulted in an increased number of incurable infections leading to a higher mortality rate, especially in hospitals. [1] Nosocomial or hospital-acquired infections are transmitted either through direct or indirect contact. [2,3] As soon as any microorganism or pathogens encounter another living organism or a surface, they tend to adhere to the host, build colonies, and form biofilms, which can be a source of further infections. [4] Therefore, the first step is to prevent transmission e.g., via isolation of the patient or extensive sanitization of the surfaces, which can be achieved with physical cleaning. However, a smarter option is to use surfaces with antibacterial and self-cleaning properties that require considerably less maintenance. [5].

The antibacterial effects of copper and its alloys have garnered significant attention in the scientific community over the past few decades. Numerous studies have been conducted to explore their potential as an antibacterial agent. [6] Recent studies [7] show that it is related to the Cu-ion release from the surface, which is responsible for the degradation of bacterial cells. [8,9] Further studies have demonstrated the formation of reactive oxygen species in the presence of copper oxide nanoparticles and hydrogen peroxide as well as other reactants. These reactive oxygen species induce oxidative stress, leading to the deterioration of bacterial cells. [10,11] Additionally, the use of ultrashort pulsed direct laser interference patterning to produce superficial structures in the dimension of the bacteria provides a larger contact area. The increased surface area enhances the bacterial killing on copper surfaces further. DLIP is a

Abbreviations: CuZn15, Brass with 15% zinc content; CLSM, confocal laser scanning microscopy; CFU, colony-forming units; *E. coli*, *Escherichia coli*; FWHM, full width at half maximum; GI-XRD, grazing incidence X-ray diffraction; HAZ, heat-affected zone; PBS, phosphate-buffered saline; SEM, scanning electron microscopy; STEM-EDS, scanning transmission electron microscopy along with energy dispersive X-rays spectroscopy; TEM, transmission electron microscopy, USP-DLIP, ultrashort pulsed direct laser interference patterning; XPS, X-ray photoelectron spectroscopy.

* Corresponding author at: Chair of Functional Materials, Department of Material Science and Engineering, Saarland University, 66123 Saarbrücken, Germany.
E-mail address: aisha.ahmed@uni-saarland.de (A.S. Ahmed).

https://doi.org/10.1016/j.apsusc.2024.160338
Received 18 December 2023; Received in revised form 20 April 2024; Accepted 19 May 2024
Available online 20 May 2024

very well-known high-speed technique for creating superficial periodic structures down to the nanoscale that are very precise and can alter the surface properties. [12] Nature is a primary example of micro- and nanoscale features in different species, demonstrating how such superficial structures have evolved over the years according to their functionalities i.e., light absorption, wettability, adhesion, friction, mechanical strength, etc. [13–16] These examples are an inspiration for DLIP method, which is used for surface modification of various materials to obtain specific properties with diverse applications. [12,17].

The DLIP technique combined with the ultrashort pulsed (USP) duration causes the matter to ablate with heat-affected zones (HAZ) only at the nano-scale. [18] In the case of copper, it leads to topographical and chemical modification of the surface, which works in favor of the antibacterial properties. [7,19] However, a recent study [20] on USP-DLIP treatment of brass with 37 % zinc shows that these nano-scale HAZ cannot be completely neglected, as they led to some major chemical modifications of the surface, i.e. not only the formation of oxide phases but also the intermetallic β-phase of brass. Therefore, a decrease in the release of copper ions is observed, which significantly reduces the antibacterial efficacy.

This study aims to investigate the correlation between the chemical modification of HAZ by USP-DLIP and the bulk chemical composition of brass and to understand its influence on antibacterial properties. While pure copper surfaces possess beneficial antibacterial properties, they also face mechanical limitations in application. Alloying, particularly with zinc, offers a feasible solution to expand applications by enhancing durability and corrosion resistance. For that purpose, commercially available brass with 15 % zinc (CuZn15) is chosen. Since it has a zinc content below 30 ± 3 wt-%, the probability of the formation of any intermetallic phases is low. [21] Given that earlier investigations [20] with elevated zinc content revealed the emergence of both intermetallic and oxide phases following USP-DLIP modification, this study aims to enhance our understanding of the consequences of preventing intermetallic phase formation on the alteration of antibacterial efficacy. In brief, periodic line-like structures in the dimension of the single bacterial cell, *Escherichia coli* (*E. coli*), are fabricated, characterized, and finally tested for their antibacterial efficacy.

2. Materials and methods

2.1. Materials

This study uses brass with 15 % zinc (CuZn15, *Wieland*) together with two references i.e., 99 % pure copper (*Wieland*), and stainless steel 304 (*Brio*). The sample sheets, each measuring approximately 1 mm in thickness, were trimmed to dimensions of around 25 x 10 mm^2 followed by a metallographic preparation as described in Ahmed *et al.* [20] to acquire a mirror-quality finish. For that purpose, the sample surface was first ground with SiC paper (15 μm grain size) on a manual Tegrapol system (*Struers*). It was then polished using an all-in-one diamond solution (Dia Duo 2 from *Struers*) on an automated TegraPol system (*Struers*), which involved three steps using the following grain sizes: 6 μm, 3 μm, and 1 μm.

2.2. Ultrashort pulsed direct laser interference patterning

Line-like structures with a periodicity of 3 μm were fabricated on the CuZn15 surface as described in Ahmed *et al.*[20] For that purpose, USP-DLIP with the following laser system and parameters was employed: a Ti:sapphire Spitfire laser system (*Spectra Physics*) with ultrashort laser pulses (pulse duration of t_p = 100 fs, full width at half maximum, FWHM) and centered wavelength $\lambda = 800$ nm. The optical configuration was selected in accordance with the description provided by Müller *et al.* [22] A fluence of 0.84 J/cm^2 with a total number of approx.10 pulses were applied to produce the structures. Following the laser treatment, the samples underwent a minimum aging period of three weeks to guarantee stable and reproducible wettability conditions. [7] For the characterization and the tests, the structured samples were observed in as-processed and etched conditions. “As-processed” denotes samples that have undergone laser processing and aging, whereas “etched” indicates structured samples immersed in a 5 % citric acid solution in an ultrasonic bath for 2 min, then cleaned with ethanol to eliminate any process-induced oxides and subsequently aged for 3 weeks.

2.3. Characterization

At first, confocal laser scanning microscopy (CLSM, *LEXT OLS4100 3D Measuring Laser Microscope by Olympus*) was utilized to verify the topography of structures followed by scanning electron microscopy (SEM, *Helios NanoLab 600™, FEI Company*) to acquire images in secondary electron contrast mode. For that an acceleration voltage of 5 kV and a current of 1.4 nA were used, whereas the sample was tilted at 45° to obtain a better image of the line-like structures. Subsequently, a quantitative phase analysis was performed via a high-resolution grazing incidence X-ray diffractometer (GIXRD, Cu K_α source with a wavelength of 1.5418 Å at 1° grazing angle, *PANalytical X'Pert PRO-MPD*). The raw data underwent processing with the X'pert HighScore software (version 5.1), [23] which encompassed baseline correction and peak identification for comparison with the database.

Scanning transmission electron microscopy also including energy-dispersive X-ray spectroscopy (STEM-EDS, JEOL ARM 200F cold FEG equipped with two Cs correctors) was applied to determine the chemical composition via mapping and profiling. Wherefore, thin foil lamellas (perpendicular to the lines) were produced by using a focused ion beam (FIB) SEM dual beam system *FEI Helios NanoLab 600i*.

The oxides characterization was carried out with X-ray photoelectron spectroscopy (XPS, Vacuum Generators ESCA MKII, non-monochromatic Al-K_α radiation (1486.6 eV), normal emission).

2.4. Antibacterial tests

Wet plating method [24] is used in this work to test the antibacterial activity on all three brass surfaces (polished, as-processed, etched) including the copper and stainless-steel references. The bacteria of strain *E. coli* WT K12 (BW25113) were used in the wet plating. The preparation of the bacterial culture was conducted following the method outlined in Luo *et al.* [6] The bacterial suspension was applied in the form of a 40 μL droplet to perform the contact-killing experiment as described in previous studies. [7,20] The experiment was carried out across three distinct durations: 30 min, 60 min, and 120 min. At the conclusion of each period, two droplets of 5 μL each were collected. One is diluted in a phosphate buffer saline (PBS) solution to then spread on an agar plate consisting of lysogeny broth (LB), which is later stored in an incubator at 37 °C. Following a 24-hour period, the total count of surviving colony units (CFU/mL) was determined. The second droplet was diluted into 600-fold of 0.1 % HNO_3 to assess the release of Cu ions during 120 min of contact. The measurement is carried out with inductively coupled plasma mass spectrometry (ICP-MS, Agilent 8900 ICP-QQQ). When evaluating the results, the increase in the contact area and the variation in wettability were taken into account as described in Ahmed *et al.* [20].

3. Results and discussion

3.1. Topographical modification

Fig. 1 shows the topography with the line-like structures on CuZn15. By subjecting the surface to ultrashort pulsed laser irradiation, high temperatures, and localized stress are generated, resulting in the material ablating in the form of a phase explosion and the ejection of molten material. [25,26] This process creates periodic line-like structures, as observed in this work where the periodicity is 3 μm and the depth is 1.3 ± 0.1 μm. The increase in surface area is 2.3-fold, with the valleys

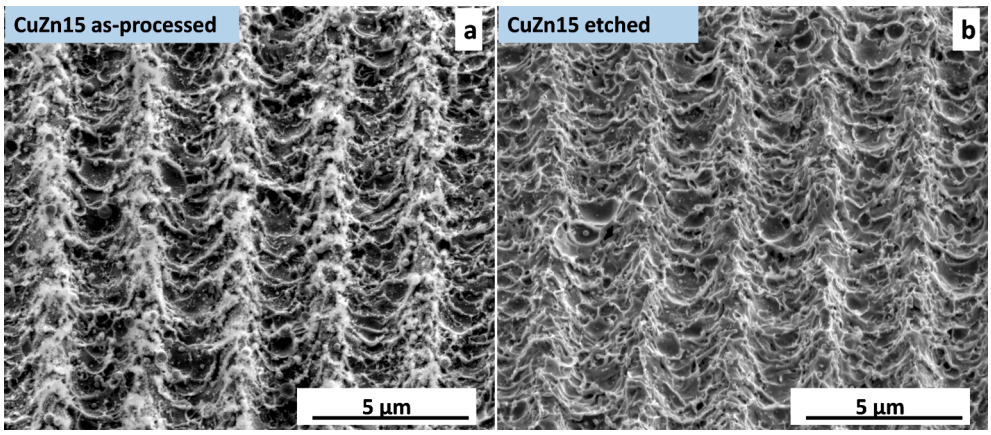

Fig. 1. SEM-images of line-like structures fabricated by USP-DLIP on CuZn15 (a) in as-processed state and (b) after etching with citric acid. The structures have a periodicity of 3 µm.

exhibiting a concave form that is approx. 2 times larger surface area than that of the peaks. Overall, the aim is to enhance the bacteria-substrate contact via this structure form.

The formation of oxides is evident in the flake-like sub-structures observed on the as-processed sample shown in Fig. 1 a. This occurrence is particularly beneficial for pure copper as it leads to a heightened antimicrobial effect by promoting corrosion and subsequently releasing more copper ions. [7] On the contrary, brass with higher zinc content experience the formation of predominantly zinc-rich phases with oxygen when irradiated with a USP laser. Correspondingly, a higher corrosion resistance is achieved resulting in lower Cu-ions release. [20].

The interaction between bacteria and the substrate is significantly influenced by the release of Cu ions and surface wettability, and both are affected by oxide formation. [6] In order to investigate the effect of oxide formation on brass with low zinc content, the surfaces were etched. This results in the removal of the flake-like sub-structures revealing the actual structure underneath (see Fig. 1 b). The structures exhibit nanoroughness along the lines, likely due to the presence of melting zones and the resulting multi-ripples. This is further aided by redepositioning the molten material as nanoparticles. The structures obtained in this study agree well with those in recent studies. [7,20].

3.2. Phase analysis

This section deals with phase analysis of brass surfaces in the polished state and after laser structuring in the as-processed and etched state. The black diffractogram in Fig. 2 shows peaks at 43°, 50°, 73.6°, 89°, 94.1°, and 115.2° that are designated characteristic peaks of an α-phase in brass with 85 wt-% copper and 15 wt-% zinc (LPF:1826484, ICDD:04–018-5556). Likewise, similar peaks with no significant distinctions are recorded for the structured surfaces. These results show no phase alteration of α-brass for CuZn15 via laser treatment. However, the SEM images (see Fig. 1) indicate the removal of flake-like sub-structures on the surface, which will be further investigated in the subsequent sections.

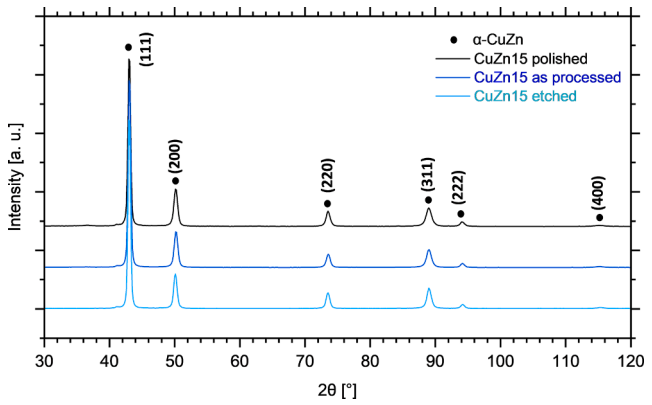

Fig. 2. Results of GI-XRD on brass with 15% zinc content: polished (black diffractogram), as-processed (dark blue diffractogram), etched (light blue diffractogram). (For interpretation of the references to color in this figure legend, the reader is referred to the web version of this article.)

3.3. Chemical modification

STEM-EDS analysis was carried out on the structured CuZn15 surfaces. To conduct the investigation, a cross-section was prepared perpendicular to the line-like structures, followed by the extraction of lamella from the prepared cross-section.

Fig. 3 illustrates the elementary mapping on a peak (tilted clockwise at 90°) of the CuZn15 as–processed sample. The map indicates unaltered chemical composition until the last 65 nm from the surface. In these last ca.65 nm towards the uppermost surface, a substantial variation in the mapping suggests a depleted copper content with an increased quantity of zinc alongside oxygen. This proposes the formation of zinc oxide through laser processing. In comparison to the GI-XRD results, no oxide phases were discernible in the XRD spectra. One potential explanation for this could be that the oxide formed in this case is of an amorphous nature, making it challenging to detect via XRD.

For further analysis, line scans containing seven points were carried out from the bulk towards the surface. The results are summarized in Table 1 showing that the values are in agreement with the bulk composition until the second last position. However, a drastic change in the composition was recorded for the last position close to the surface. Here, the copper content is reduced from about 84 to 27 at-%. In parallel, an increase is recorded for zinc from about 14.5 to 57 at-% as well as for oxygen from a negligible value to 15.5 at-%. Hence, the occurrence of oxides on the surface is confirmed. The chemical composition suggests the formation of a mixture of zinc and copper oxides. Excluding oxygen, the Cu/Zn atomic ratio on the topmost surface is now approx. 0.48.

Additionally, the chemical composition of CuZn15 etched is shown in Table 2 The results show a decrease in oxygen content from 15.5 to 8.7 at-% implying a successful, but partial removal of oxides through etching. Simultaneously, the reduction in zinc and oxygen confirms the formation of a zinc-rich oxide layer through laser structuring. The preferential formation of zinc oxide is related to the fact that zinc requires, comparatively, lower Gibbs energy change for the oxide formation.[27].

As the new layer is revealed after etching, it now has a Cu to Zn

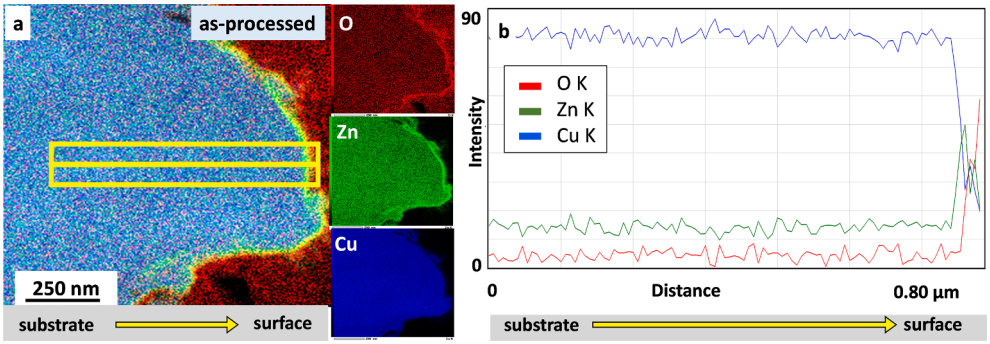

Fig. 3. Results of STEM-EDS mapping on as-processed CuZn15: (a) color elemental map of a peak (clockwise rotation at 90°, substrate (left) to surface (right)); (b) the intensity profile of the yellow line scan in a). (For interpretation of the references to color in this figure legend, the reader is referred to the web version of this article.)

Table 1
Results of STEM-EDS on CuZn15 as-processed.

Distance from the surface [nm]	at-%		
	Cu	Zn	O
709	84.8	14.5	0.7
592	84.8	14.4	0.8
475	83.9	14.9	1.2
358	84.3	14.6	1.1
242	85.6	14.3	0.1
125	84.2	14.6	1.2
0	27.3	57.2	15.5

Table 2
Results of STEM-EDS on CuZn15 etched.

Distance from the surface [nm]	at-%		
	Cu	Zn	O
509	84.8	14.3	0.9
426	84.7	14.6	0.7
339	84.9	14.4	0.7
256	84.8	14.3	0.9
175	83.6	14.7	1.7
85	84.0	15.0	1.0
0	66.4	24.9	8.7

atomic ratio of about 2.7 indicating a copper-rich uppermost layer (see Table 2). Fig. 4 shows the TEM-EDS map and profile of an etched sample and as it is compared with the profile of the as-processed sample in Fig. 3, it shows that a few tens of nanometers has been removed from the surface through etching. The elevated thermal and kinetic energy near the surface, induced by laser irradiation, plays a key role in facilitating the diffusion of copper and zinc atoms in the subsurface, providing an explanation for this occurrence. As the sample is etched and the zinc-rich phase with oxygen is removed, the inner layer into which the copper has diffused becomes visible.

3.4. Characterization of oxide phases

In this section, XPS analysis combined with surface ablation by Ar-ion etching is utilized to further investigate the chemical composition as well as the oxidation state of Cu and Zn at the surface and subsurface levels.

First, XPS-based elemental depth profiles are recorded and the results are displayed in Fig. 5 a. Here, the two horizontal reference lines represent the bulk concentration (in at-%) for copper (orange) and zinc (blue). The as-processed CuZn15 sample shows a reduced content of copper and an equally increased concentration of zinc towards the surface. The same effect is visible on the etched sample. However, the depth of this variation is significantly less. This is connected to the presence of oxygen on the subsurface of the samples (see Fig. 5 b and c), which is deeper for the as–processed samples. For the as-processed sample, the nearly 1: 1 ratio of Cu and Zn in Fig. 5 a is not in contrast to Table 1 where an enrichment of Zn is observed. In Table 1 the increase of Zn content is observed at the peak positions of the line structures while in Fig. 5 the XPS data display intensities as averaged over nearly 1 cm^2. These distinctions are likely attributable to the uneven distribution of chemical composition at the ten-nanometer range.[20] Nevertheless, the commonality lies in the increase of zinc content in the modified surface area relative to the bulk composition.

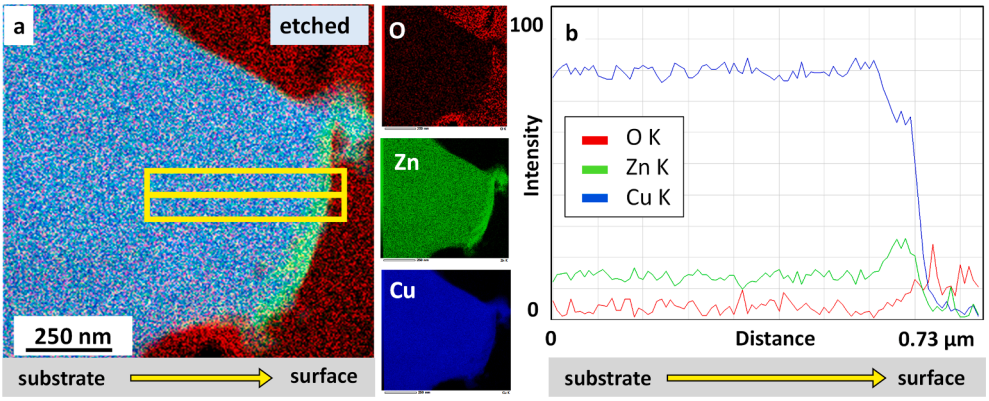

Fig. 4. Results of STEM-EDS mapping on etched CuZn15: (a) color elemental map of a peak (clockwise rotation at 90°, substrate (left) to surface (right)); (b) the intensity profile of the yellow line scan in a). (For interpretation of the references to color in this figure legend, the reader is referred to the web version of this article.)

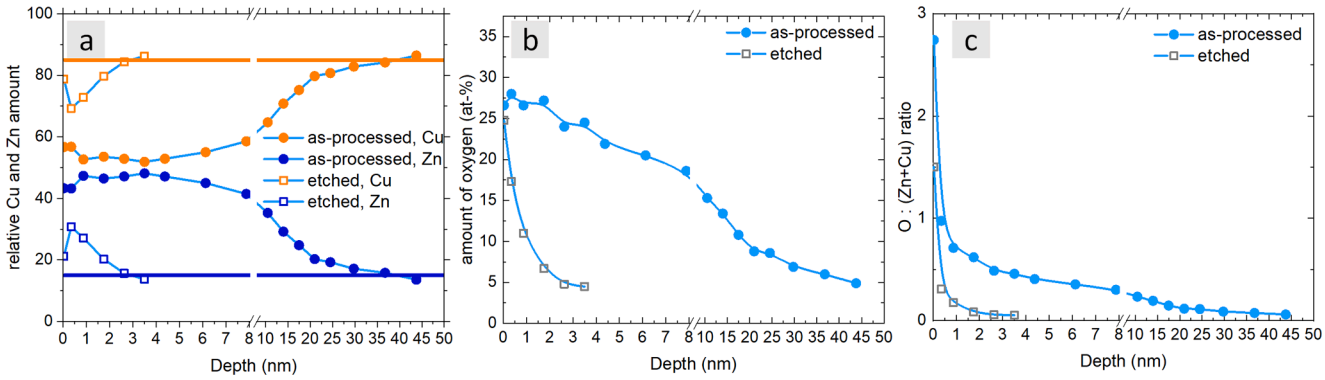

Fig. 5. (a) Atomic Cu:Zn ratio (b) amount of oxygen in at.% and (c) atomic O:(Zn + Cu) ratio as obtained by elemental depth profiling in XPS for CuZn15.

The survey data of the as-received samples (i.e., before Ar ion ablation) showed the presence of Cu, Zn, and O (as well as C from adsorbates). For quantitative analysis (i.e., distribution of elements, oxidation state of Zn and Cu), high-resolution spectra were recorded for O 1 s, Cu 2p, Zn 2p, Cu LMM, and Zn LMM. The analysis approach was the same as described in Ahmed *et al.* [20] In the Cu-2p spectra in Fig. 6 a and b contributions from Cu and Cu_2O cannot be distinguished. However, CuO differs from Cu and Cu_2O by two spectral features. For CuO, there is a shift to higher binding energy and there is the characteristic satellite at higher binding energy. [28–31] Contributions from Cu can be distinguished from contributions of Cu_2O and CuO by the low binding energy part (approx. 565 eV) of the $L_3M_{45}M_{45}$ peak in the Cu-LMM spectra in Fig. 6 c and d. Zn-2p spectra in general display no characteristic features to distinguish Zn from ZnO. Contributions from Zn and ZnO can be distinguished by the differences in peak shape and peak position in the Zn-LMM spectra in Fig. 6 e and f. [28,32,33].

Fig. 6 a shows the Cu-2p spectra for the CuZn15 (as-processed) sample as well as for Cu and CuO reference samples. In the initial state (no Ar ion etching, ablation 0 nm), the double Cu-$2p_{3/2}$ and Cu-$2p_{1/2}$ peaks as well as the CuO-like satellites ($Sat_{3/2}$, $Sat_{1/2}$) predict contributions of CuO and Cu/Cu_2O. After ablation of only 0.35 nm, no spectral features of CuO are visible, i.e. there is e.g. a single Cu-$2p_{3/2}$ peak at 932.4 eV as representing Cu and/or Cu_2O. [28,32] Since the thickness of the ablated surface layer is in the range of atomic distances in Cu or Cu oxides, the absence of any CuO-related spectral features gives evidence that the formation of CuO only affects the 1–2 outmost atomic layers. Fig. 6 c illustrates the Cu LMM spectra compared to the spectra from Cu and CuO reference samples. For Cu_2O the reference spectrum is taken from Fig. 5 in Schedel *et al.* [30] (since the spectra for Cu and CuO shown there are very similar to the spectra of Cu and CuO as probed with our setup). In the as-provided state (0 nm) and after ablation of 0.35 nm, the spectra display a superposition of the Cu, Cu_2O, and CuO spectra. At further ablation (i.e., $\geq$ 0.88 nm) the Cu contribution starts to increase (see e.g., the Cu-characteristic peak at 565 eV), and with each new step of ablation, the spectra adapt more and more the Cu reference data. According to Fig. 6 a and c, CuO is present only at the surface (and maybe the subsurface layer) while Cu_2O is distributed only up 3–4 nm into the bulk.

Fig. 6 e shows the Zn LMM spectra for CuZn15 in the as-processed state. When compared to spectra as probed on ZnO and Zn reference samples it is evident that ZnO is distributed much deeper into the bulk than CuO and Cu_2O. Even after an ablation of approx. 44 nm the Zn-LMM spectrum still represents a superposition of Zn and ZnO. The amount of ZnO exceeds the amount of Zn in depths ranging down to 15 nm. Below 15 nm the amount of Zn starts to dominate but even in the deepest bulk range that was probed (i.e., approx. 44 nm) the Zn LMM spectrum still displays contributions from ZnO. Compared to the distribution of CuO and Cu_2O, the distribution of ZnO in Fig. 5 c and Fig. 6 e evidently show that Zn traps oxygen. This is also supported by the amount of oxygen in Fig. 5 b that is distributed in line with the amount of Zn in Fig. 5 a.

After etching CuZn15 samples with citric acid, the chemical composition of the surface and the subsurface regime is strongly different. Fig. 5 b shows a significant decrease in the oxygen content. In Fig. 6 b nearly no CuO-related satellite is visible in the Cu-2p spectrum for zero ablation, i.e., there is nearly no CuO even at the surface. The Cu-LMM in Fig. 6 d shows that there is also no large contribution of Cu_2O in the subsurface regime. Only at the surface (0 nm ablation), the Cu-LMM displays an overlap of the Cu and Cu_2O reference data, but at 0.35 nm ablation, the Cu-LMM spectrum strongly resembles the spectrum of the Cu reference sample. After etching, ZnO is still present in the bulk. However, the Zn-LMM spectra in Fig. 6 f show that the contributions of ZnO are strongly reduced in comparison to the as-processed sample. The amount of ZnO is much strongly reduced with increasing depth as in the case of the as-processed sample. This is shown by e.g., the comparable weak ZnO-related peak intensities at 498 eV in comparison to the Zn-related peak intensities at about 495 eV. In the Zn-LMM spectrum of CuZn15 etched at about 3.50 nm ablation in Fig. 6 f shows that the ZnO-related peak is smaller as in the Zn-LMM spectrum of CuZn15 as-processed at about 43.75 nm ablation in Fig. 6 e. Etching of the CuZn15 sample therefore results in a decrease of the thickness of the (mainly) ZnO layer by more than one order of magnitude. As observed in comparison with the STEM-EDS results, it is evident that a layer measuring a few tens of nanometers has been removed from the surface through etching.

The findings indicate the presence of cupric oxide primarily at the topmost layer, while the formation of zinc oxide and cuprous oxide occurs in the underlying layers beneath the surface. Additionally, the much higher concentration of zinc throughout the modified thickness and towards the upper surface of CuZn15 as-processed suggests an asymmetrical diffusion. Therefore, a non-equilibrium transport of the lattice is observed, where the diffusion of the zinc atoms towards the surface is significantly faster than the diffusion of the copper atoms away from the surface. This phenomenon is commonly known as the Kirkendall effect.[34] After etching, there is a decrease in the levels of zinc and oxygen, leading to the emergence of a copper-rich oxide phase. This observation implies the partial elimination of the zinc oxide phase.

3.5. Antibacterial tests

This section is concerned with the results of contact killing tests on brass with 15 % zinc (CuZn15). In total, three different surfaces of CuZn15 in the polished, as-processed, and etched state were tested, along with mirror-polished copper and stainless steel as references.

Fig. 7 a exhibits the surviving CFU/mL values over a contact period of 120 min for all samples. Furthermore, these results are complemented by the corresponding release of Cu-ions after 120 min (see the bars in Fig. 7 b). The references show an expected antibacterial behavior i.e.,

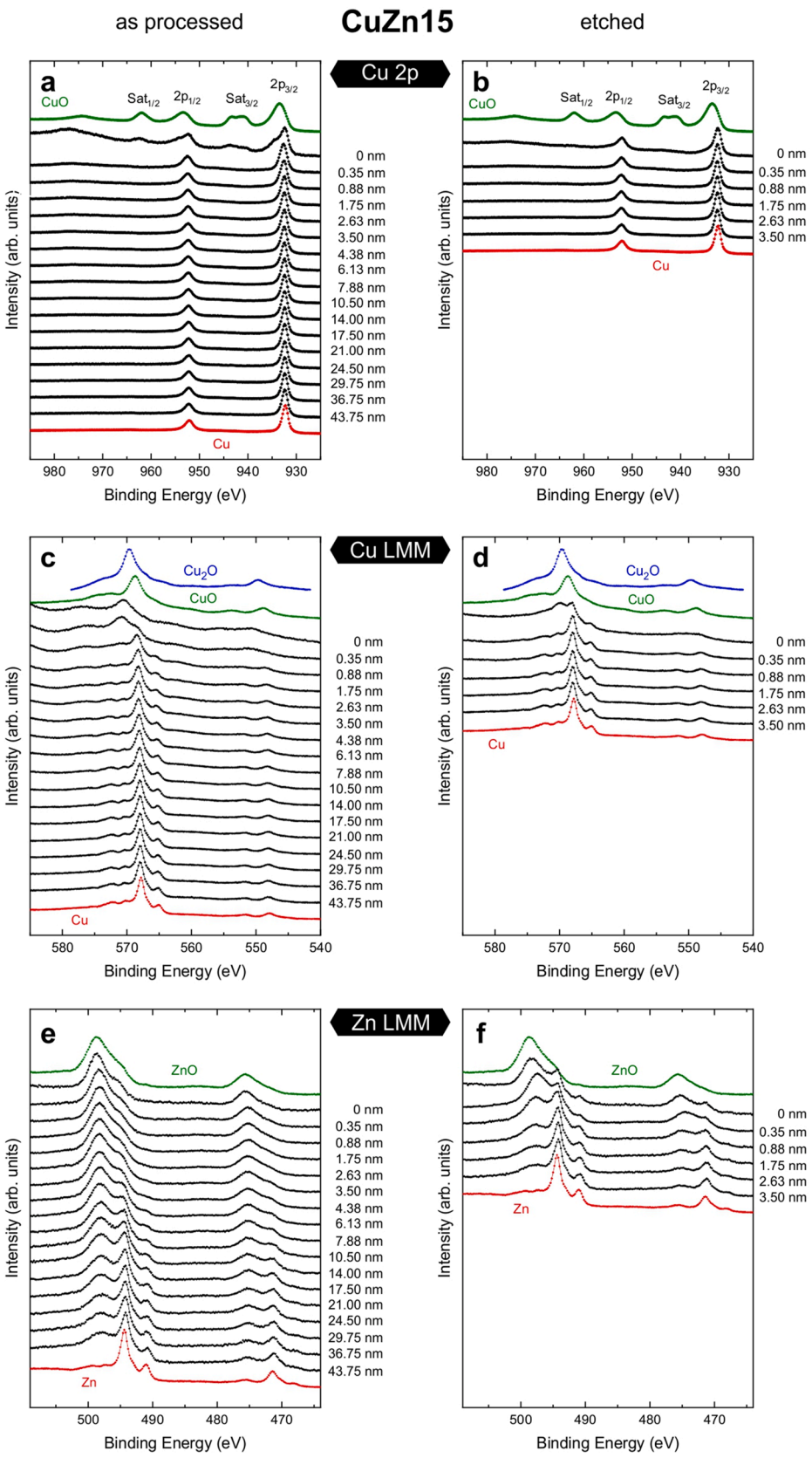

Fig. 6. High-resolution XPS-spectra of (a, b) Cu 2p, (c, d) Cu LMM and (e, f) Zn LMM of as-processed (a, c, e) and etched samples (b, d, f), respectively. This also includes the reference spectra for CuO (green), Cu_2O (dark blue), Cu (red), ZnO (green) and Zn (red). (For interpretation of the references to color in this figure legend, the reader is referred to the web version of this article.)

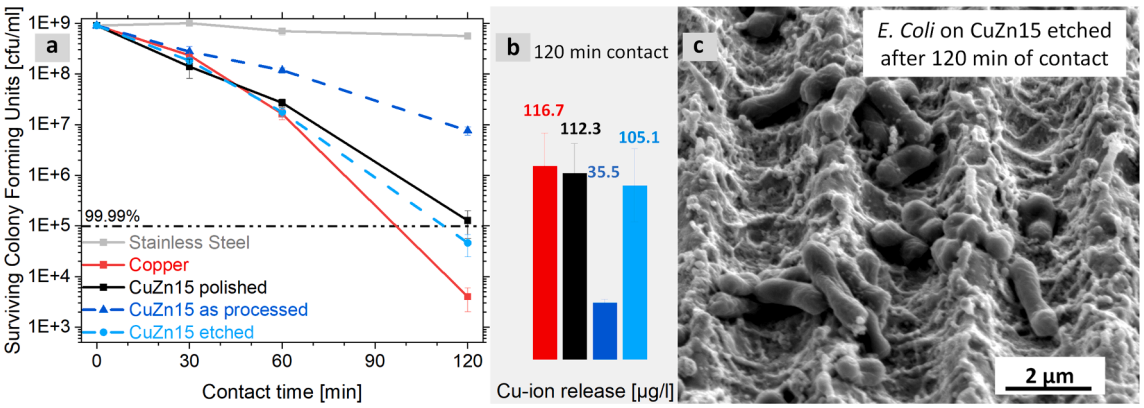

Fig. 7. Results of contact killing experiment with *E. coli*: (a) Surviving colony-forming units for 30, 60 and 120 min on reference surfaces (steel and copper) and all three CuZn15 surfaces (polished, as-processed and etched). (b) The Cu-ion release values at 120 min are represented in form of a bar chart. (c) SEM image of *Escherichia coli* in the line-like structures of the etched CuZn15 surface. The image was taken at 52° tilt.

the poor killing of *E. coli* by stainless steel (grey) and an excellent one by the copper surface (red). [7,20] Simultaneously, the polished CuZn15 (black) displays a similar behavior until the first 60 min of exposure as compared to the copper reference. However, in the following 60 min, it shows a relatively reduced killing of *E. coli*. This can be attributed to the lower concentration of copper in brass,[6,35] which was validated by the slightly reduced Cu-ion release concentration after 120 min. Meanwhile, a drastic change in antibacterial behavior is observed for the as-processed CuZn15 (dark blue). In the initial 60 min of contact, the number of surviving CFU/mL is one magnitude higher compared to the polished brass surface. However, with the increasing exposure time, the killing rate on the as-processed surface is attenuated resulting in a bigger difference. This is attributed to the fact that the copper content has reduced by half (as also shown by STEM-EDS results), which explains the lowered Cu-ions release and thence decreased killing of *E. coli.* At the same time, the zinc content has increased. A previous study suggests an antibacterial effect of ZnO nanostructures on *E. coli*, attributed to the release of zinc ions under UV irradiation. [36] However, the experiments in this study were conducted on bulk material under ambient conditions, and there are no studies demonstrating an antibacterial effect of zinc without UV irradiation. However, etching the surface results in an improved efficiency, which in the case of CuZn15 etched (light blue graph in Fig. 7 a) is instantly better than that of polished CuZn15 (black graph). This can be attributed to the removal of the unwanted oxide layer, exposing the layer beneath with more favorable conditions to release copper ions. It is to be noticed that the Cu-ion release for the etched sample is similar to that for the polished and yet the killing on the etched surface is enhanced. This is a possible result of the topographical modification, which is further examined in the next section.

3.6. State of surface after bacteria-substrate contact

Fig. 7 c displays the bacterial-substrate contact, revealing that the bacteria mainly reside in the valleys of the structures. This contact results in a significant alteration of both the surface and the bacteria. In order to investigate this further, a comparison of the surface topography was conducted before and after contact with the bacteria. Fig. 8 a and c illustrate the surface prior to contact with *E. coli*, showing a rapid cooling of the melted material along with the redeposition of ablated material in the form of round nanoparticles, as well as smooth surface areas in between.

After contact with the bacteria (Fig. 8 b and d), the surface exhibits nano roughness, which is indicative of corrosion and subsequent release of Cu ions. This effect is particularly prominent in the valleys. Furthermore, the Cu ion release observed for the etched surface (light blue) in Fig. 7 a is comparable to that of polished CuZn15 (black). This suggests that the improved ability to kill *E. coli* on the etched surface is due to both the release of copper ions and the surface's topography.

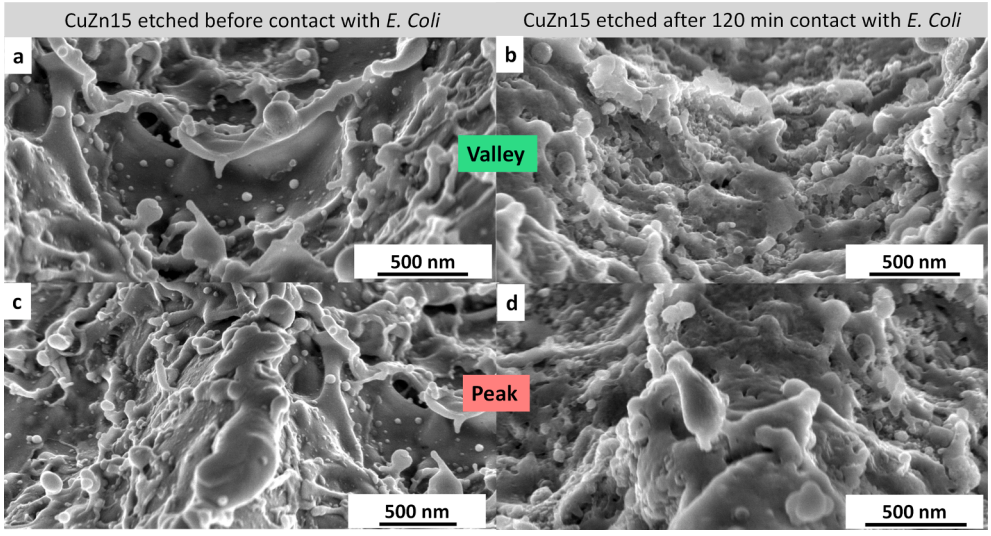

Fig. 8. SEM images of the etched CuZn15 surface exhibiting valley and peak of line-like structures each (a, c) before and (b, d) after 120 min contact with *E. coli*. The images were taken at 52° tilt.

Chemical analysis was conducted using SEM-EDS to further examine the samples. The results in Fig. 9 b show that the peak (red, position 2 in Fig. 9 a) contains higher zinc and oxide content compared to the valley (green, position 1 in Fig. 9 a). This might explain why the peaks have greater resistance to corrosion in the bacterial solution with PBS and experience less alteration on their surfaces after coming into contact with bacteria. However, further investigations need to be done to determine the corrosion resistance of the brass surface modified via DLIP.

When the bacteria are taken under observation one interesting aspect noticed here is the presence of nano agglomerates on the cell membrane (see Fig. 9 a). These agglomerates were identified as part of the bacterial cell membrane upon closer examination (magnified in the yellow circle in Fig. 9 a). This is potentially associated with the penetration of Cu-ions into the bacterial cells. To investigate the chemical composition of these agglomerates, SEM-EDS analysis was conducted (see position 3, pink spectra in Fig. 9 b). However, it should be noted that the characterization method has limitations, and therefore the results may also contain information from the substrate beneath the bacteria. The exact interaction mechanism between ions and bacteria still remains inconclusive. However, previous studies [8,9,37] suggest that when the cell membrane is ruptured, there is a leakage of intracellular components leading to the death of bacterial cell. Alternatively, there is a chance that before cell membrane rupture, copper ions deposit onto the membrane and are subsequently absorbed into the cell through respiratory processes. These Cu-ions are likely to react with these components as well as DNA, leading to the formation of copper complexes. These complexes hinder any potential repair processes, contributing to the eventual deterioration of bacterial cells.

To further observe the bacteria-substrate contact, FIB cross-sections were performed perpendicular to the line-like structures containing *E. coli*. Fig. 10 a shows that the bacterium on the right side exhibits strong adhesion, with the bacterial cell membrane appearing to merge with the substrate. On the left, the bacterium has detached a portion of the surface, revealing underlying surface corrosion. Furthermore, backscattered electron (BSE) imaging was utilized to detect the contrast between bacteria with different chemical compositions. In Fig. 10 b, the BSE image shows varying contrasts within the bacteria. Bacterium no. 1 displays no contrast, while bacterium no. 2 exhibits a uniform distribution of brighter and darker zones. Bacterium no. 3 exhibits the most distinct contrast between the inner part of the bacterium and the nano agglomerates formed within the cell membrane. The presence of copper, which is a heavier element than other elements in the chemical composition of *E. coli*, may cause it to appear brighter in the image. By comparing the FIB-SEM and BSE images, it is evident that different bacteria are likely in different stages of adhesion and contact with Cu-ions. To gain a better understanding of these phenomena, further investigation methods will be necessary for future studies.

4. Conclusion

This study investigates and compares the importance of zinc content in brass for surface modification using USP-DLIP to previous studies. A chemical composition with zinc content lower than 30 ± 3 wt-% was chosen to lower the possibility of the formation of intermetallic phases in brass. As expected, the only chemical modification observed is the formation of oxide phases. The results reveal a profound modification on a nanoscale, with a significant presence of zinc oxide in both superficial and subsurface layers.

After laser processing, the reduced copper content in the brass leads to a slower killing rate compared to a polished brass sample. However, after etching, the amount of zinc oxide decreases, followed by the complete removal of cupric oxide from the uppermost layer. This exposes a copper-rich layer, resulting in a higher release of Cu-ions and consequently a higher killing rate of *E. coli* on the etched brass with 15 % zinc compared to the polished brass sample.

The SEM images and EDS analysis suggest an alteration of the surface as well as bacteria upon contact with each other. It is noticeable that the valleys have a higher level of corrosion in the presence of bacterial solution with PBS compared to the peaks. This difference in corrosion may be attributed to the higher zinc and oxide content in the peaks, i.e., possibly higher corrosion resistance, which needs to be investigated in future. The bacteria, on the other hand, show the formation of nano agglomerates on their cell membrane. This indicates a possible presence of Cu-ions in the bacteria, as also suggested by the BSE imaging. The findings suggest that the enhanced antibacterial activity is attributed to a higher quantitative bacteria-substrate contact accompanied by a higher Cu-ion release. However, further investigations using high-resolution methods are needed to fully understand the bacteria-substrate interaction and the killing mechanism of Cu-ions. Additionally, exploring other etching solutions can help remove zinc oxide fully from the structured surfaces and analyze its impact on the bacteria-substrate contact.

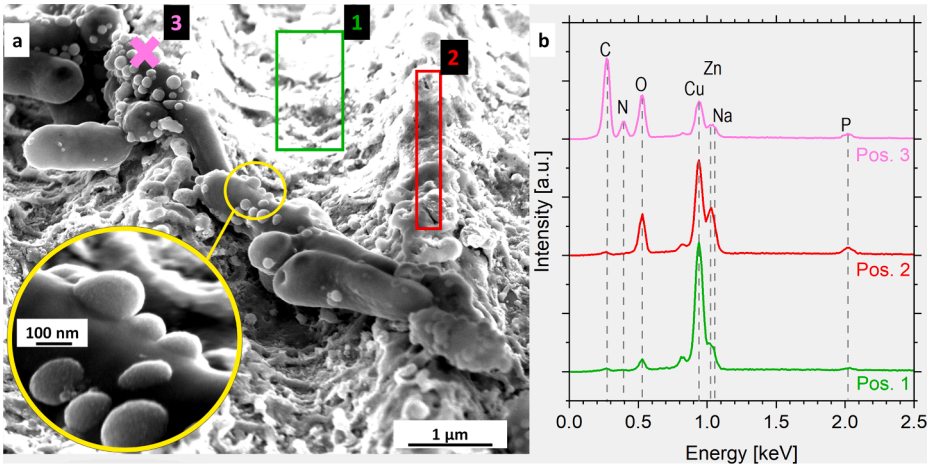

Fig. 9. (a) SEM image of *E. coli* on the structured and etched CuZn15 surface after two hours exposure time. The yellow circle represents the position of magnified image of the bacteria with nano agglomerates. The squares and cross shape show the position of EDS measurements. The images were taken at a tilt of 52°. The corresponding EDS spectra are displayed in (b). (For interpretation of the references to color in this figure legend, the reader is referred to the web version of this article.)

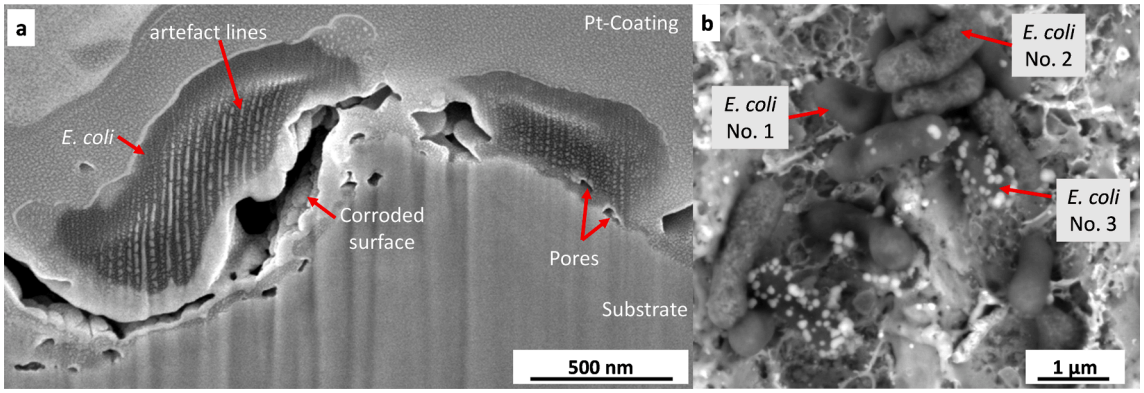

Fig. 10. (a) SEM image of bacteria on substrate. The FIB cross section was done perpendicular to the line-like structures. The artefact lines in the bacteria are a result of FIB cross section. (b) BSE image of *E. coli* on CuZn15 etched.

CRediT authorship contribution statement

Aisha Saddiqa Ahmed: Conceptualization, Investigation, Validation, Visualization, Writing – original draft. **Daniel Wyn Müller:** Investigation, Validation, Writing – review & editing. **Stéphanie Bruyère:** Investigation, Validation, Writing – review. **Anne Holtsch:** Investigation, Validation, Writing – review & editing. **Frank Müller:** Investigation, Validation, Writing – review & editing. **Kristina Brix:** Investigation, Validation, Writing – review. **Sylvie Migot:** Investigation. **Ralf Kautenburger:** Supervision. **Karin Jacobs:** Writing – review & editing, Supervision. **Jean–François Pierson:** Writing – review & editing, Resources, Supervision. **Frank Mücklich:** Funding acquisition, Resources, Supervision.

Declaration of competing interest

The authors declare that they have no known competing financial interests or personal relationships that could have appeared to influence the work reported in this paper.

Data availability

Data will be made available on request.

Acknowledgments

The Author would like to thank to the group of Prof. Rolf Müller from the Helmholtz Centre of Infection Research in Saarbrücken for providing the *E. coli*. The authors would like to thank the technical platforms “Microscopies, Microprobes and Metallography (3 M)” and “Optic and Lasers” at Institut Jean Lamour (IJL, Nancy, France) for access to FIB and TEM facilities.

References

[1] CDC, Antibiotic Resistance Threats in The United States 2019, Cdc 10 (2019). doi: https://doi.org/10.15620/cdc:82532.
[2] A.U.M. Khan, A. Torelli, I. Wolf, N. Gretz, AutoCellSeg: Robust automatic colony forming unit (CFU)/cell analysis using adaptive image segmentation and easy-to-use post-editing techniques, Sci Rep 8 (2018), https://doi.org/10.1038/s41598-018-24916-9.
[3] K.A. Davis, J.J. Stewart, H.K. Crouch, C.E. Florez, D.R. Hospenthal, Methicillin-resistant Staphylococcus aureus (MRSA) nares colonization at hospital admission and its effect on subsequent MRSA infection, Clinical Infectious Diseases 39 (2004) 776–782, https://doi.org/10.1086/422997.
[4] R.M. Donlan, Biofilm formation: A clinically relevant microbiological process, Clinical Infectious Diseases 33 (2001) 1387–1392, https://doi.org/10.1086/322972.
[5] J. Hasan, R.J. Crawford, E.P. Ivanova, Antibacterial surfaces: The quest for a new generation of biomaterials, Trends Biotechnol 31 (2013) 295–304, https://doi.org/10.1016/j.tibtech.2013.01.017.
[6] J. Luo, A. Ahmed, J.F. Pierson, F. Mücklich, Tailor the antibacterial efficiency of copper alloys by oxidation: when to and when not to, J Mater Sci 57 (2022) 3807–3821, https://doi.org/10.1007/s10853-022-06879-5.
[7] D.W. Müller, S. Lößlein, E. Terriac, K. Brix, K. Siems, R. Moeller, R. Kautenburger, F. Mücklich, Increasing Antibacterial Efficiency of Cu Surfaces by targeted Surface Functionalization via Ultrashort Pulsed Direct Laser Interference Patterning, Adv Mater Interfaces 8 (2021), https://doi.org/10.1002/admi.202001656.
[8] M. Raffi, S. Mehrwan, T.M. Bhatti, J.I. Akhter, A. Hameed, W. Yawar, M.M. Ul Hasan, Investigations into the antibacterial behavior of copper nanoparticles against Escherichia coli, Ann Microbiol 60 (2010) 75–80, https://doi.org/10.1007/s13213-010-0015-6.
[9] G. Tong, M. Yulong, G. Peng, X. Zirong, Antibacterial effects of the Cu(II)-exchanged montmorillonite on Escherichia coli K88 and Salmonella choleraesuis, Vet Microbiol 105 (2005) 113–122, https://doi.org/10.1016/J.VETMIC.2004.11.003.
[10] F.A. Bezza, S.M. Tichapondwa, E.M.N. Chirwa, Fabrication of monodispersed copper oxide nanoparticles with potential application as antimicrobial agents, Sci Rep 10 (2020), https://doi.org/10.1038/s41598-020-73497-z.
[11] C. Angelé-Martínez, K.V.T. Nguyen, F.S. Ameer, J.N. Anker, J.L. Brumaghim, Reactive oxygen species generation by copper(II) oxide nanoparticles determined by DNA damage assays and EPR spectroscopy, Nanotoxicology 11 (2017), https://doi.org/10.1080/17435390.2017.1293750.
[12] A.F. Lasagni, C. Gachot, K.E. Trinh, M. Hans, A. Rosenkranz, T. Roch, S. Eckhardt, T. Kunze, M. Bieda, D. Günther, V. Lang, F. Mücklich, Direct laser interference patterning, 20 years of development: from the basics to industrial applications, in: Laser-Based Micro- and Nanoprocessing XI, SPIE, 2017: p. 1009211. doi: 10.1117/12.2252595.
[13] X. Li, G.S. Cheung, G.S. Watson, J.A. Watson, S. Lin, L. Schwarzkopf, D.W. Green, The nanotipped hairs of gecko skin and biotemplated replicas impair and/or kill pathogenic bacteria with high efficiency, Nanoscale 8 (2016) 18860–18869, https://doi.org/10.1039/c6nr05046h.
[14] K. Liu, L. Jiang, Bio-inspired design of multiscale structures for function integration, Nano Today 6 (2011) 155–175, https://doi.org/10.1016/j.nantod.2011.02.002.
[15] R.J. Crawford, E.P. Ivanova, S.H. Nguyen, H.K. Webb, Natural Superhydrophobic Surfaces, Superhydrophobic Surfaces (2015) 7–25, https://doi.org/10.1016/B978-0-12-801109-6.00002-1.
[16] E. Arzt, H. Quan, R.M. McMeeking, R. Hensel, Functional surface microstructures inspired by nature – From adhesion and wetting principles to sustainable new devices, Prog Mater Sci 120 (2021) 100823, https://doi.org/10.1016/J.PMATSCI.2021.100823.
[17] F. Rößler, V. Lang, D. Günther, A.F. Lasagni, Fabricating Three-Dimensional Periodic Micro Patterns on Photo-Resists Using Laser Interference Lithography, Adv Eng Mater 19 (2017), https://doi.org/10.1002/adem.201600855.
[18] J. Bonse, J. Krüger, Probing the heat affected zone by chemical modifications in femtosecond pulse laser ablation of titanium nitride films in air, J Appl Phys 107 (2010), https://doi.org/10.1063/1.3311552.
[19] D.W. Müller, A. Holtsch, S. Lößlein, C. Pauly, C. Spengler, S. Grandthyll, K. Jacobs, F. Mücklich, F. Müller, In-Depth Investigation of Copper Surface Chemistry Modification by Ultrashort Pulsed Direct Laser Interference Patterning, Langmuir 36 (2020) 13415–13425, https://doi.org/10.1021/acs.langmuir.0c01625.
[20] A.S. Ahmed, D.W. Müller, S. Bruyere, A. Holtsch, F. Müller, J. Barrirero, K. Brix, S. Migot, R. Kautenburger, K. Jacobs, J.-F. Pierson, F. Mücklich, Surface Modification of Brass via Ultrashort Pulsed Direct Laser Interference Patterning and Its Effect on Bacteria-Substrate Interaction, ACS Appl Mater Interfaces (2023), https://doi.org/10.1021/acsami.3c04801.
[21] P. Kejzlar, J. Machuta, I. Nová, Comparison of the Structure of CuZn40MnAl Alloy Casted into Sand and Metal Moulds, Manufacturing Technology 17 (2017) 15, https://doi.org/10.21062/ujep/x.2017/a/1213-2489/MT/17/1/44.
[22] D.W. Müller, T. Fox, P.G. Grützmacher, S. Suarez, F. Mücklich, Applying Ultrashort Pulsed Direct Laser Interference Patterning for Functional Surfaces, Sci Rep 10 (2020), https://doi.org/10.1038/s41598-020-60592-4.

[23] T. Degen, M. Sadki, E. Bron, U. König, G. Nénert, The high score suite, Powder Diffr (2014), https://doi.org/10.1017/S0885715614000840.
[24] E.R. Sanders, Aseptic laboratory techniques: Plating methods, Journal of Visualized Experiments (2012) 1–18, https://doi.org/10.3791/3064.
[25] L.V. Zhigilei, B.J. Garrison, Microscopic mechanisms of laser ablation of organic solids in the thermal and stress confinement irradiation regimes, J Appl Phys 88 (2000) 1281–1298, https://doi.org/10.1063/1.373816.
[26] J.E. Masse, G. Barreau, Laser generation of stress waves in metal, Surf Coat Technol 70 (1995) 231–234, https://doi.org/10.1016/0257-8972(95)80020-4.
[27] M. Hasegawa, Ellingham Diagram, Treatise on, Process Metallurgy 1 (2014) 507–516, https://doi.org/10.1016/B978-0-08-096986-2.00032-1.
[28] S. Poulston, P.M. Parlett, P. Stone, M. Bowker, Surface oxidation and reduction of CuO and Cu2O studied using XPS and XAES, Surface and Interface Analysis 24 (1996) 811–820, https://doi.org/10.1002/(SICI)1096-9918(199611)24:12<811::AID-SIA191>3.0.CO;2-Z.
[29] D. Barreca, A. Gasparotto, E. Tondello, CVD Cu2O and CuO Nanosystems Characterized by XPS, Surface Science Spectra 14 (2007) 41–51, https://doi.org/10.1116/11.20080701.
[30] T. Schedel-Niedrig, T. Neisius, I. Böttger, E. Kitzelmann, G. Weinberg, D. Demuth, R. Schlögl, Copper (sub)oxide formation: A surface sensitive characterization of model catalysts, Physical Chemistry Chemical Physics 2 (2000) 2407–2417, https://doi.org/10.1039/b000253o.
[31] L. Armelao, D. Barreca, M. Bertapelle, G. Bottaro, C. Sada, E. Tondello, A sol–gel approach to nanophasic copper oxide thin films, Thin Solid Films 442 (2003) 48–52, https://doi.org/10.1016/S0040-6090(03)00940-4.
[32] J.P. Tobin, W. Hirschwald, J. Cunningham, XPS and XAES studies of transient enhancement of Cu1 at CuO surfaces during vacuum outgassing, Applications of Surface Science 16 (1983) 441–452, https://doi.org/10.1016/0378-5963(83)90085-5.
[33] F. Wiame, F.R. Jasnot, J. Wiatowska, A. Seyeux, F. Bertran, P. le Fèvre, A. Taleb-Ibrahimi, V. Maurice, P. Marcus, Oxidation of α-brass: A photoelectron spectroscopy study, Surf Sci 641 (2015) 51–59, https://doi.org/10.1016/j.susc.2015.05.013.
[34] E.O. Kirkendall, Diffusion of zinc in alpha brass, Trans. Am. Inst Min. Metall 147 (1942) 104–110.
[35] S. Mehtar, I. Wiid, S.D. Todorov, The antimicrobial activity of copper and copper alloys against nosocomial pathogens and Mycobacterium tuberculosis isolated from healthcare facilities in the Western Cape: an in-vitro study, Journal of Hospital Infection 68 (2008) 45–51, https://doi.org/10.1016/j.jhin.2007.10.009.
[36] R. Goyal, P. Roy, P. Jeevanandam, Antibacterial activity studies of ZnO nanostructures with different morphologies against E, in: Coli and S. Aureus, Appl Phys A Mater Sci Process 129, 2023, https://doi.org/10.1007/s00339-023-06530-3.
[37] J. Luo, C. Hein, J. Ghanbaja, J.F. Pierson, F. Mücklich, Bacteria accumulate copper ions and inhibit oxide formation on copper surface during antibacterial efficiency test, Micron 127 (2019), https://doi.org/10.1016/j.micron.2019.102759.